2D PIC-MCC code for electron-hydrogen gas interaction study in H^- ion sources

Karim Benmeziane [(1)(2)], Robin Ferdinand[(1)], Raphael Gobin[(1)], Gerard Gousset[(2)]

(1) Commissariat l'Energie Atomique, CEA-Saclay, DSM/DAPNIA, 91191 Gif sur Yvette Cedex, France
(2) Laboratoire de physique des gaz et des plasmas (Associ au CNRS), 91405 Orsay cedex, France

Abstract: In order to make a reliable H^- ion source, a hybrid PIC 2D MCC 3D [1] fluid code has been developed. The aim of the code is to study the effect of electron injection into a cylindrical gas chamber. This new version takes into account the 2D space charge distribution. Thus, it is possible to calculate the H^- ion distribution everywhere in the plasma chamber. Many results have been brought as well as the best injected energy and the electron penetration length efficiency. Moreover, the calculations explain why it is more problematic to get an efficient volume production at high pressure (100 mTorr) than at low pressure (6 mTorr). The temporal H^- production evolution is finally discussed.

INTRODUCTION

Few years ago started experimental investigation on an ECR H^- ion source at CEA-Saclay. Many results have been brought [2,3,4]. Conclusions have been carried, but questions are still remaining. The ECR H^- ion source would not produce current more intense than a few µA if it kept as simple ECR source. The high frequency wave creates high-energy electrons not efficient for negative ions production. Moreover this source has the advantage to generate a high electron density current, then a high proton current has been currently measured. It is understandable regarding of these sources origin. They have been used to perform hard X ray, or larges concentrations of proton [5]. Among all sources previously working all around the world, two groups can be distinguished. Those working via a surface processes and volume processes. It is thus possible to bring this source to one of these groups. The choice has been pointed on a volume processes. Surface process is very efficient only if cesium addition is preceded. This element brings the wall material work function down. It is then easy to capture electrons on the surface by atoms.

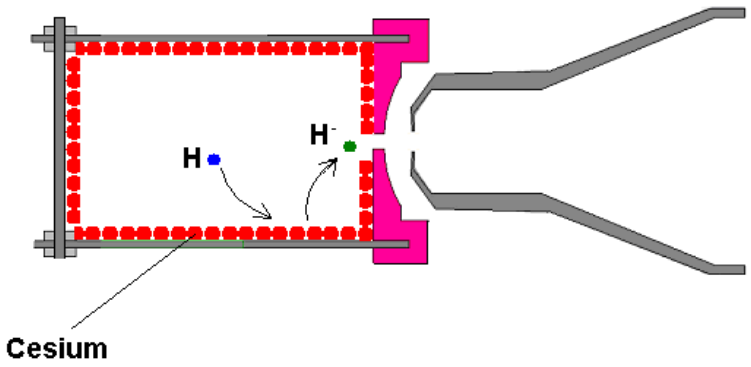

Figure 1:Cesium seeding effect

The studied ECR source procuresses a large amount of hydrogen atoms. It would be a very good H^- ions production surface source if the emphasis were not laid on a long lifetime. On contrary large source of atoms are not desired for H^- volume production study.
ECR ion sources have an important advantage, which is their long lifetime in continuous running mode. Nowadays, Filament source like give important current of H ion. Thus, the idea is to use the ECR source as an electron source. The beam extracted from the source is supposed to be injected into a second chamber which is actually the same gas chamber just separated by a grid system. Those electrons would relax their energy, heat the plasma but no microwave is required in this second chamber. For many years, the process leading to H^- ion is getting well known. It is called the dissociative attachment (D-A) [6]

$$e_{slow} + H_2(v>9) \rightarrow H + H^- .$$

Such reactions have a threshold zero for vibrational levels larger than nine. Then, it is essential to have hydrogen molecules in a vibrational state higher than 9 with large density. To make them (most of $H_2(v>9)$), electrons with energies around 20 eV are needed. To obtain an efficient source of H^- ions, injecting electron in a hydrogen gas chamber appears to be a good solution. For these reasons a stainless steel grid with 5 mm mesh gap has been introduced in the source and huge improvement have been observed. It is then possible to move that grid at different position. This structure is supposed to stop the microwave energy. It is also possible to polarize the grid. A double grids system is expected to improve the electron injection into the second chamber. Many other applications of the grid would be brought. It is thought to build a grid in a magnetic material to decrease the effect of the transversal magnetic field in that second chamber. It would have the effect of an electron filter generally used in such a sources. A transversal magnetic field is used to avoid fast electrons in the production zone (only slow electrons are desired in this zone for the D-A). If a grid were made of a magnetic material an inductive magnetic field would appear. This field is in the so called ‘driver zone’ and is not wanted in the second chamber.

CALCULATION DESCRIPTION

To enlarge the understanding, a PIC 2D MCC3D code has been developed. The aim of the code is to understand phenomena under the interaction between an electron beam and hydrogen gas in the H^- production chamber, and especially if there is a specific place where the H^- ions are produced inside the chamber. Injecting an electron beam into a chamber is not as easy as it seems. The system becomes anisotropic which makes it quite totally different from other type of sources more symmetric (multicusps). To overcome the anisotropies configurations it is obligatory to favor a particle technique instead of a Boltzmann code generally supposes a weak anisotropy. The code is articulated in two parts: The Monte Carlo code with collision (MCC) associated with a PIC code and a ‘Fluid code’. The MCC consists in creating electrons with an initial energy on the front edge of the second chamber. The PIC code is in charge of calculating the space charge field, which forces the movement of charged particles. The second kind of code named here ‘fluid code’ is used to determine the vibrational excitation H_2 molecules and get the H^- production rates.

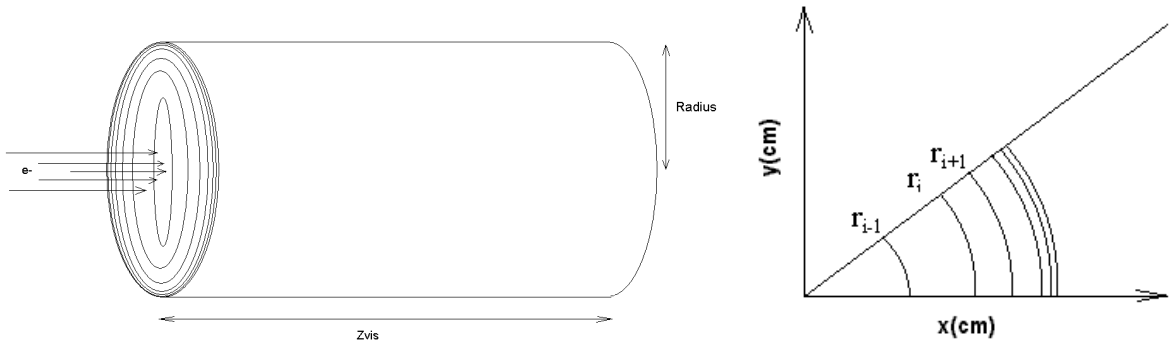

Figure 2:Diagram of the simulation status at the left. Initially the chamber radius was 1cm and the length 5cm. The electron beam is also 1cm radius. At the right is shown the radial mesh.

The MCC code keeps track of electron and their interaction with the gas including 27 processes: two rotational excitations, three vibrational excitations, four triplet state excitations, eight singlet state excitations. These processes are all described in the Table 1 and 2.

Process	Reaction	Threshold reaction (eV)
Elastic collision	$e + H_2 \rightarrow e + H_2$	0
rotational excitation	$e + H_2 (X^1\Sigma_g^+, v=0, j=0) \rightarrow e + H_2 (X^1\Sigma_g^+, v=0, j=2)$	0.044
rotational excitation	$e + H_2 (X^1\Sigma_g^+, v=0, j=1) \rightarrow e + H_2 (X^1\Sigma_g^+, v=0, j=3)$	0.073
vibrational excitation	$e + H_2 (X^1\Sigma_g^+, v=0) \rightarrow e + H_2 (X^1\Sigma_g^+, v=1)$	0.516
vibrational excitation	$e + H_2 (X^1\Sigma_g^+, v=0) \rightarrow e + H_2 (X^1\Sigma_g^+, v=2)$	1.0
vibrational excitation	$e + H_2 (X^1\Sigma_g^+, v=0) \rightarrow e + H_2 (X^1\Sigma_g^+, v=3)$	1.46
Electronic excitation $b^3\Sigma_u^+$	$e + H_2 (X^1\Sigma_g^+) \rightarrow e + H_2 (b^3\Sigma_u^+)$	10.0
Electronic excitation $c^3\Pi_u$	$e + H_2 (X^1\Sigma_g^+) \rightarrow e + H_2 (c^3\Pi_u)$	12.3
Electronic excitation $a^3\Sigma_g^+$	$e + H_2 (X^1\Sigma_g^+) \rightarrow e + H_2 (a^3\Sigma_g^+)$	12.0
Electronic excitation $e^3\Sigma_u^+$	$e + H_2 (X^1\Sigma_g^+) \rightarrow e + H_2 (e^3\Sigma_u^+)$	13.22
Electronic excitation $B^1\Sigma_u^+$	$e + H_2 (X^1\Sigma_g^+) \rightarrow e + H_2 (B^1\Sigma_u^+)$	12.7
Electronic excitation $C^1\Pi_u$	$e + H_2 (X^1\Sigma_g^+) \rightarrow e + H_2 (C^1\Pi_u)$	12.4
Electronic excitation $E^1\Sigma_g^+$-$F^1\Sigma_g^+$	$e + H_2 (X^1\Sigma_g^+) \rightarrow e + H_2 (E^1\Sigma_g^+ - F^1\Sigma_g^+)$	13
Electronic excitation $B'^1\Sigma_u^+$	$e + H_2 (X^1\Sigma_g^+) \rightarrow e + H_2 (B'^1\Sigma_u^+)$	14.8
Electronic excitation $D^1\Pi_u$	$e + H_2 (X^1\Sigma_g^+) \rightarrow e + H_2 (D^1\Pi_u)$	14.9
Electronic excitation $B''^1\Sigma_u^+$	$e + H_2 (X^1\Sigma_g^+) \rightarrow e + H_2 (B''^1\Sigma_u^+)$	15.5
Electronic excitation $D'^1\Pi_u$	$e + H_2 (X^1\Sigma_g^+) \rightarrow e + H_2 (D'^1\Pi_u)$	15.6
Ionization	$e + H_2 \rightarrow 2e + H_2^+$	15.4

Table 1:Chemistry of the PIC code, two rotational excitation, three vibrational excitation, four triplet state excitation, eight singlet state excitation, one ionization [7, 8].

Process	Branching ratio
$H_2(b^3\Sigma_u^+) \rightarrow H(1s) + H(1s)$	$\chi=1$
$H_2(c^3\Pi_u) \rightarrow H(1s) + H(1s) + h\nu$	$\chi=1$
$H_2(a^3\Sigma_g^+) \rightarrow H(1s) + H(1s) + h\nu$	$\chi=1$
$H_2(e^3\Sigma_u) \rightarrow H(1s) + H(1s) + h\nu$	$\chi=1$
$H_2(D^3\Pi_u) \rightarrow H(1s) + H(2l)$	$\chi=0.298$
$H_2(B''^1\Sigma_u^+) \rightarrow H(1s) + H(2l)$	$\chi=0.967$
$H_2(D'^1\Pi_u) \rightarrow H(1s) + H(2l)$	$\chi=1$

Table 2: Processes used to calculate hydrogen atoms by dissociation.

Excitation, ionization and dissociation are thus considered. Two types of positive ions are included in the present model. H_3^+ and H_2^+ ion kinetics are especially very fundamental ion studies when low energy are involved:

$H_2 + H_2^+ \rightarrow H_3^+ + H + 1.71eV$

To determine the relative importance of atomic positive ion concentration created by ionization of atoms, we take into account the kinetic of atoms, their volume creation and their loss at the walls. Atomic hydrogen are thus very important in the global kinetic of the system and are considered as shown on the equation above. Their loss takes place at the wall recombination giving hydrogen molecules:

$H(1s) + wall \rightarrow (1/2)H_2 (X^1\Sigma_g^+, v=0)$ ($\gamma=10^{-2}$) [9],

γ depends on the wall material (for iron [10] $\gamma=10^{-4}$, for stainless steel [11] $0.07 \leq \gamma \leq 0.15$). As result of the model prediction, the concentration of H atoms is too low to have a large concentration of H^+ ions by electron ionization. The $\frac{[H]}{[H_2]}$ order of magnitude can be under 10^{-2}. Moreover, due to the low energy of electrons the dissociation ionization by electron impact of H_2 molecules is also inefficient. Thus, H^+ ions production can be considered as negligible. Electron's cross section data of mechanisms considered in the present calculation are from two sources, J.Loureiro [12] for low kinetic energy and H.Tawara [13] for higher energy than 40 eV.

To determine the electron rate coefficient involved in the vibrational H_2 molecule kinetics, it is necessary to have some informations on electron energy distribution function 'EEDF'. The MCC code permits to have an estimation of EEDF in energy mesh as:

$$f_e(E) = \frac{n_e(r,t)}{\Delta V.\Delta E}.$$

Where n_e, ΔV, ΔE are the number of electrons and the volume, and the energy width of each cell, respectively. According the last definition, the function fe(E) is normalized to the local electron density $n_e(r,t)$. This function is thus the number of electrons per unit volume with energy between E-ΔE and E+ΔE (in eV). In the H^- ion source community it is well know that negative ion production is related with the incident power. Actually this power depends on the discharge current which itself is related with the electron density owing to the following expression: $I=e.n_e.v$, where v is the electron drift velocity.

As it is not possible to consider the movement of each electron, the use of computing techniques is necessary. To do the most of the calculation time, each computed particle so called ‘macro-particle’ or ‘super-particle’ is actually considered as many real particles (Bundle of particles) with a specific weight larger than 1. Thus, the number of calculated ‘macroparticle’ can be reduced and the number of real particles considered in the physics can be high. If this weight initially injected becomes too large, no-charge space compensation would appear and causes wrong calculation. To avoid such difficulties the weight is then gradually introduced for stability convenience of the code. This number is calculated from the following exponential function: $Weight(t) = FW*(1-e^{-t/\tau})$.
FW is the final weight to be achieved. The choice of this final weight is very important. If this factor is too large, time step will be too short and calculation time increases considerably divergences could appear. An ideal one seems to be 10^5 real particles in a ‘macro-particle’.

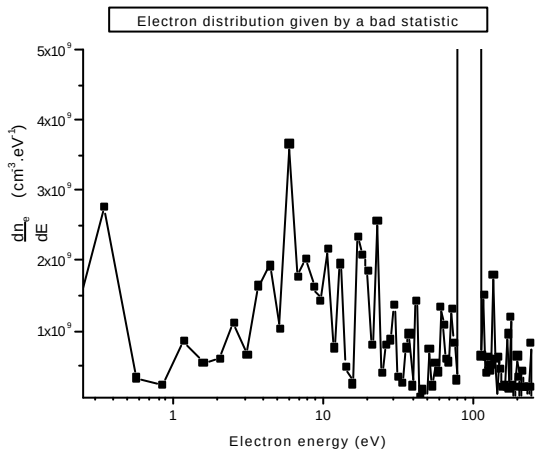

Figure 3:Bad eedf statistic given by a 10^7 weight

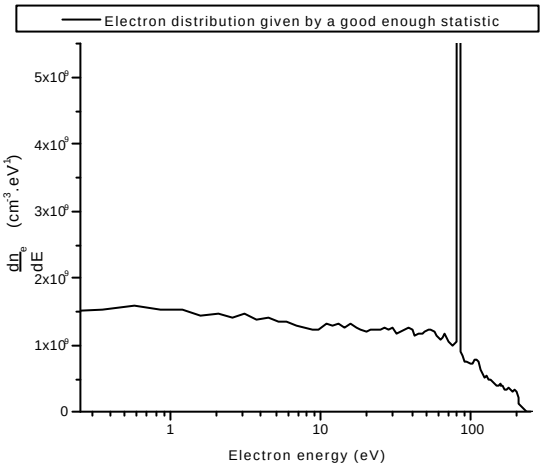

Figure 4: Reasonable statistic obtained by 10^5 weight.

The Figure 3 compared to the Figure 4 show how this is important. The EEDF have been calculated at the same plasma conditions. For the first distribution: 10^7 particles per ‘macroparticle’ are injected when they are only 10^5 in the second one. Indeed, if the weight got down the calculation precision would be better but the calculation time increases considerably. Calculation time is the only weakness of such a code, usually very reliable. This weight is a compromise between expected precision and short calculation time.
A PIC code has been used to determine the charge space field by solving the Poisson equation every 10^{-11}s which is the Maxwell time :

$$\frac{1}{r}.\frac{\partial r.E_r}{\partial r}(r,z,t)+\frac{\partial E_z}{\partial z}(r,z,t)=\frac{e.(n_+-n_e)}{\varepsilon_0}$$

It is thus possible to calculate the electric field, which forces and modifies charge particle motion all over the chamber. The calculation is completed through a spatial discretization, which is constant along z-axis but varies along radius to maintain a constant ring area (Figure 2)

THE FLUID CODE

As result of the first part of the code, the electron rate coefficient of the reactions involving the $H_2(v)$ molecules kinetic are calculated in the second part of the model.
This second part is a heavy particle kinetic code called fluid code in the rest of this paper to shortcut. This code is in charge of calculating the vibrational molecule distribution and their transports. The H^- ion production is then calculated. H^- ions are created thanks to the dissociative attachment process previously described. H_2 molecules in the vibrational states are necessary to obtain a large source rate for H^- ions. This part includes four of the dominant processes such e-V, E-V, V-T V-V.
All vibrationnal excitation source terms are described in the Table 3.

Reaction	Name
$e + H_2(w) \underset{\leftarrow}{\rightarrow} e + H_2(v)$	e-V
$e + H_2(v) \rightarrow e + H_2((B^1,C^1\Pi_u))$ $\rightarrow e + H_2(X^1\Sigma_g,v') + h\nu$	E-V
$H_2 + H_2(v+1) \underset{\leftarrow}{\rightarrow} H_2 + H_2(v)$	V-T Molecular contribution
$H + H_2(v) \underset{\leftarrow}{\rightarrow} H + H_2(v+k)$	V-T Atomic contribution
$H_2(w-1) + H_2(v+1) \underset{\leftarrow}{\rightarrow} H_2(w) + H_2(v)$	V-V

Table 3: Vibrational molecule excitation processes with each coefficient

Once all source terms have been calculated, vibrational molecules can be considered by solving the master equation. The global source term is composed by a sum of all processes source term. It gives the floowing transport equation.

$$\left(\frac{\partial N_v}{\partial t}\right)_{e-V} + \left(\frac{\partial N_v}{\partial t}\right)_{E-V} + \left(\frac{\partial N_v}{\partial t}\right)_{V-T}^{m} + \left(\frac{\partial N_v}{\partial t}\right)_{V-T}^{a} + \left(\frac{\partial N_v}{\partial t}\right)_{V-V} = div\vec{\Gamma}_{H2}$$

This equation can be solved by a Rung-Kutta method respecting the boundary conditions. Those conditions are mainly a flux equal to zero at the center, and the Miles condition at the edge.

$$\Gamma_H(r=R) = \frac{g_H.N_{H2}.\alpha_H.v_{mH}}{4(1-g_H/2)}$$

This last condition is initially a condition for atoms, but it can be adapted for molecules knowing that $\Gamma_H = -2.\Gamma_{H2}$. The Miles condition becomes: $\Gamma_{H2(v)}(r=R) = -\frac{1}{2}.\frac{g_H.N_{H2}.\alpha_H.v_{mH}}{4(1-g_H/2)}$.

The H^- ion calculation gets possible thanks to a balance equation [14]:

$$N_{H-} = \frac{n_e \sum_{v=0}^{v=14} N_v C_{att}(v)}{n_e.K_{rec} + N_H.K_{\det} + \frac{1}{t_d}}$$

$$C_{att}(v) = \int f_e(E).v_e(E)\sigma_{ad}(v,E)dE$$

The above equation has been used to obtain the results presented in this paper first part. The second part takes into account H- transport which is obviously not done by the formula above.

K_{rec} is the H^- ion recombination coefficient. It is corresponding to the losses term for the reaction:
$H^- + ions \rightarrow neutrals \quad K_{rec} = 2\ 10^{-7}\ cm^3.s^{-1}$
K_{det} and K_e are H^- ion detachment coefficient with hydrogen atoms and electrons respectively. The first one is corresponding to the losses term for the reaction:
$H^- + H \rightarrow H_2 + e \quad K_{det} = 1.8\ 10^{-9}\ cm^3.s^{-1}$
The second process corresponds to:
$H^- + e \rightarrow H + 2e \quad K_e = 7.6\ 10^{-9}\ cm^3.s^{-1}$
It is clear that atoms are very important to give a realistic calculations. Among all particles involved the excited molecule calculation atome play an important role. Thus, atoms are not only calculated in the PIC-MCC but some of them are determined thanks to the fluid code. Even if atoms from the H_3^+ conversion ($H_2 + H_2^+ \rightarrow H_3^+ H + 1.71eV$) are most another type of atoms calculation are integrated by including an additional dissociation branch. It is the dissociation from the vibrational level number 15, all other molecules below this threshold give H considering the conditions previously introduced. This vibrational dissociation is modeled as shown below:
$H_2(15) + e \rightarrow H + H^* + e$,
$H_2(15) + H \rightarrow H + H^* + H$
$H_2(15) + H_2 \rightarrow H + H^* + H_2$
Each $H_2(15)$ molecules calculated automatically give two atoms.

RESULTS AND DISCUSSION

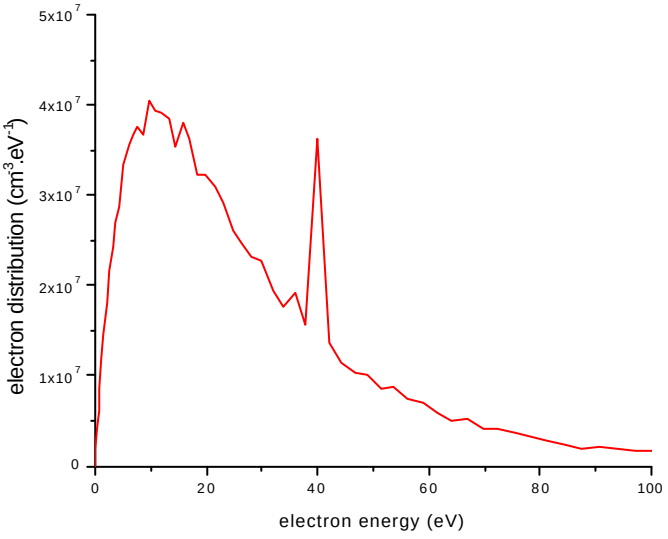

Figure 5: eedf obtained by injecting 40 mA electron beam at 40 eV in 100 mTorr of hydrogen gas.

For a start a 1D PIC has been developed, with an assumption based on electric fields negligible along the z-axis. A first calculation has been performed for 40 mA of 40 eV electron beam injected in 100 mTorr pressure hydrogen gas chamber at a temperature of 300 K. The EEDF obtained after two days calculation is represented on the Figure 5. The

EEDF tail spreads over 40 eV and denotes the electron acceleration due to the space charge. This is typically the electron energy distribution function used to determine the vibrational distribution.

Vibrational molecule calculation on the Figure 6 seems to be satisfying. The distribution converges at 0.146 ms corresponding to calculation times previously given. At 0.089 ms, the atomic population is not set yet [11]. It is due to non-equilibrium between E-V processes and atomic V-T. This effect gets compensated after 0.125 ms.

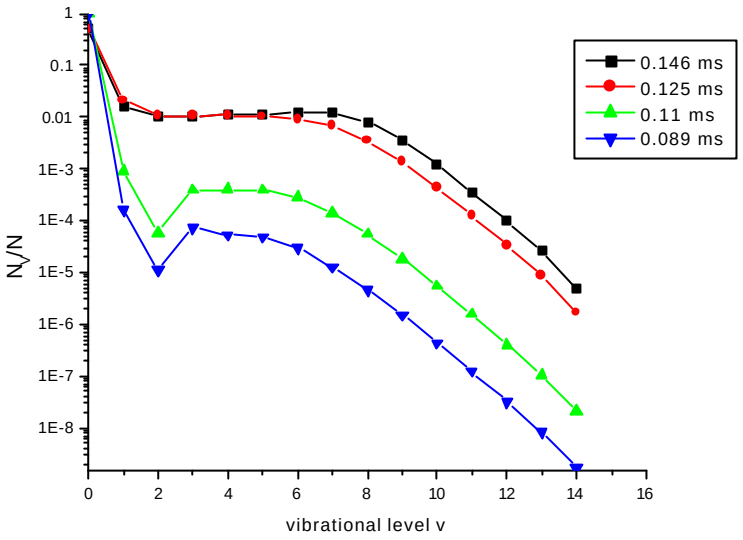

Figure 6: Evolution of the eedf with the time at 100 mTorr with a 40 mA electron beam at 40 eV.

The electron energy distribution function and the vibrational distribution are known at every point of the chamber. It is then possible to calculate the H ion source rate profile in 2D space even if the H ions transport is not done. For ion sources development, we can point out the source rate profile for negative ions. This profile is represented in Figure 7 by the ratio: H ion source term over the term of losses.

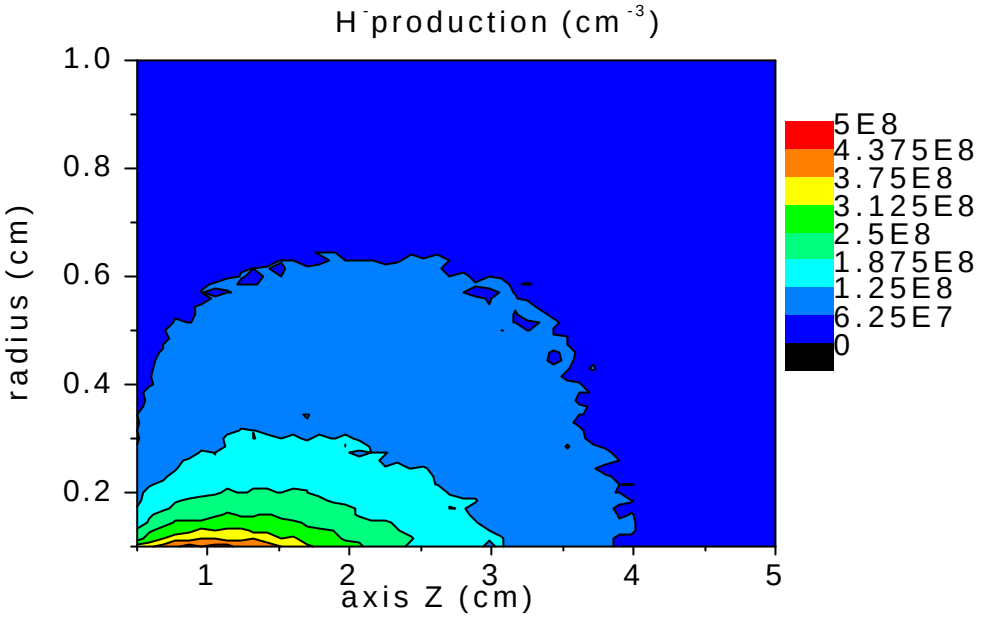

Figure 7: Distribution of H ions production in 2D view for 40 mA electron beam of 40 eV injected in a hydrogen gas chamber at a pressure of 100 mTorr. The H- transport has also been calculated and no big different are noticed.

The maximum H⁻ ion production is spread up to 2 or 3 cm. It actually shows the electron efficiency through the z-axis. It also has been demonstrated by the Nietzche code [15] that H⁻ ions are destroyed 3 cm from the origin point they took place.

At the same time experimental measurements aimed to injected electrons into a second chamber confirm this result. This experiment consists to introduce a polarized stainless grid inside an ECR ion source to control the energy of the injected electrons. The maximum current is measured when the grid is placed between 2 and 3cm form the extraction electrode. A grid at 3 cm seems to be better. The experimental result is exposed at the end of this paper on the Figure 15. The Figure 8 shows how H^- ion production and electron are related, which is quite expected considering the equation used to calculate the H ion production. This result confirms the idea that 100 mTorr is a too high pressure for the H⁻ ion production. For such a source a ratio of 2.3 10^{-2} is too small to be acceptable.

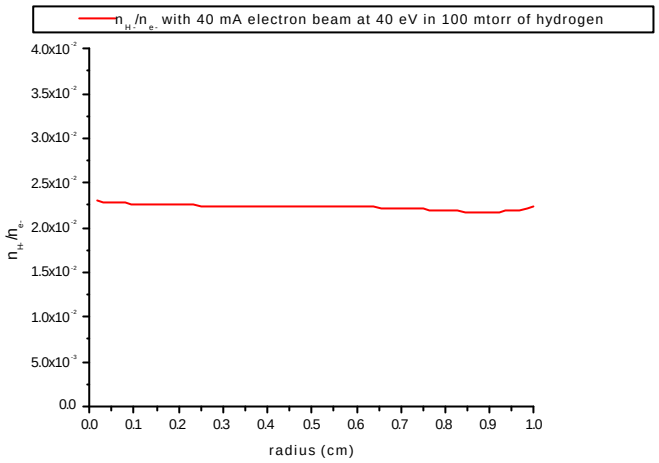

Figure 8: Average value of H^- ions over electron density ratio along the radius.

Results previously showed are obtained at 100 mTorr. At this pressure, many reasons can intervenes in the low H^- ion concentration. This pressure carries more atomic hydrogen and consequently brings a high destruction level. This plasma configuration increases the ionization and raises the mutual neutralization, which is a reason of H^- lose. Every efficient H^- ion source works at a very low pressure (between 1 and 10 mTorr) because of the pumping system, that is another reason why it is interesting to be able to get the pressure down.

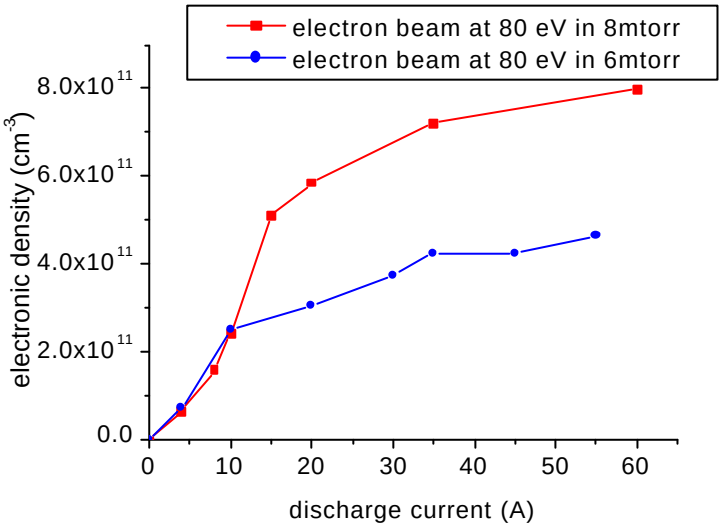

Figure 9: Electron density as a function of the current discharge for 6 and 8 mTorr by injecting electron beam at 80 eV.

Many difficulties are coming with this purpose of reducing the pressure. Decrease the pressure has the consequence to increase the free mean path of electron. If one wants a reasonable number of events taking place inside the chamber, it is important to enlarge it. For instance reducing the pressure by a factor of ten involves an enlargement of radius by a factor of $\sqrt{10}$. If so, cells areas become ten times bigger. Important consequences on the stability of the Poisson equation would be noticed. To keep cells size at the same dimension one has to increase cells number by a factor of 10. In that case the calculation time would be affected. To work this out, the solution is to include a solenoidal magnetic field in the calculation. For the

moment a constant magnetic field equal to 1200 Gauss [16] is considered. It is in consequence, possible to achieve a pressure down to 6 mTorr. The Figure 9 shows how relevant are the results obtained for 6 and 8 mTorr since it has already been measured with filament source at the same conditions.
The analysis of the Figure 7 obviously reveals that H^- space distribution is not homogeneous. The non-existent electric field along the z-axis hypothesis is not correct. It has been then decided to solve the Poisson equation in two dimensions.

FIRST RESULTS FOR THE 2D CALCULATION

Very promising results are obtained after having adapted the 1D code to a 2D PIC. In additional an H^- transport routine makes the calculation more realistic. One can observe a real improvement of the EEDF with the time (Figure 10) and can compare this curve with the one displayed on the Figure 4. Both are obtained in the same condition. The plasma thermalization goes a lot quicker in the 2D version (Figure 4). This improvement is characterized by a 2D EEDF magnitude higher at low energy range and inferior at higher range than 80 eV (the EEDF spreading reduces at high energy).

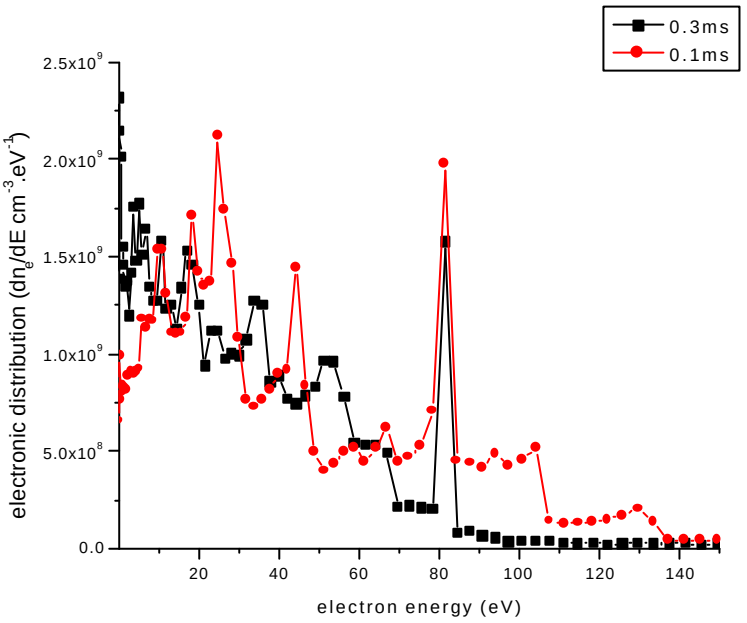

Figure 10: Evolution of the electron energy distribution function with the time at 6 mTorr with a 10 A electron beam at 80 eV.

The vibrational distribution function is very satisfying as presented on the Figure 11:

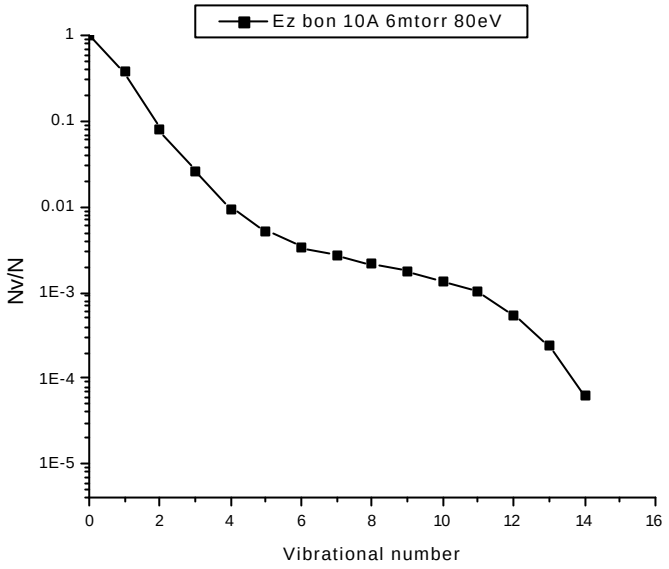

Figure 11: Vibrational distribution for 10 A of electron beam at 80 eV in 6 mTorr.

One can denote that is very important to get an idea about the most valuable energy. It is then possible to proceed to a comparison of the H ion production for different electron energy beams. Here the H^- transport has been calculated by using an exponential schema [17] to solve the equation: $\mathrm{div}\Gamma_{H^-} = S_{H^-}$. The source term is:

$$S_{H^-} = n_e.K_{rec}.N_{H^-} + N_H.N_{H^-}.K_{\det} + \frac{N_{H^-}}{t_d} - n_e.\sum_{v=0}^{v=14} N_v.C_{att}(v)$$

The energy range around 40 eV appears to be the most efficient

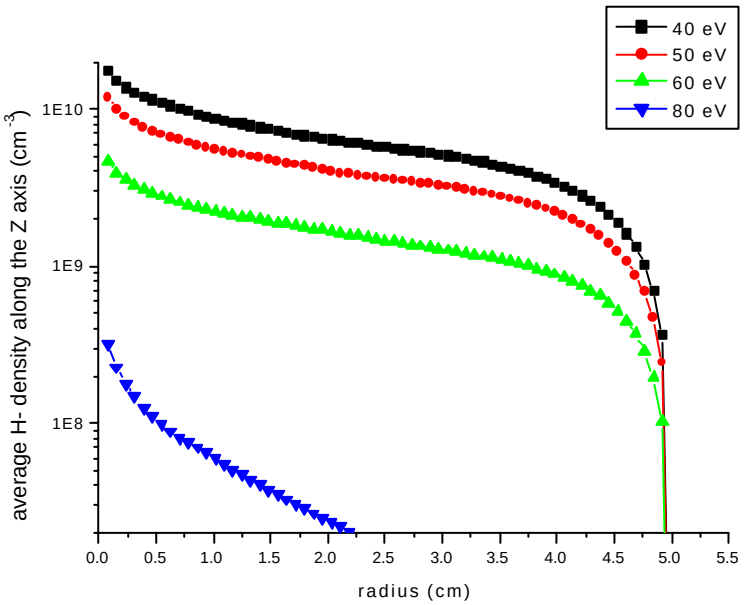

Figure 12: average H- density at 0.3 ms for 10 A electron beam at 80 eV

The H⁻ over electron ratio, gives a probably the best idea of the efficiency of the electron. Injecting electrons at around 40 eV allows the best H^- ion density as possible.

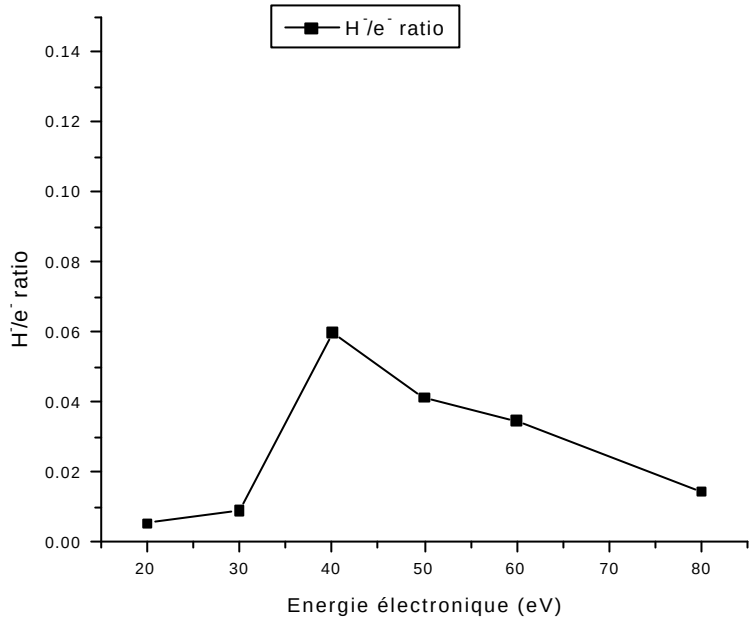

Figure 13: H^-/e^- ratio for 10 A electron beam 6 mTorr for different energy.

ELECTRON PENETRATION EFFICIENCY

As shown in the Figure 14 the electron penetration is efficient along around 3 cm. The calculation has been later confirmed by measurements presented the Figure 15.

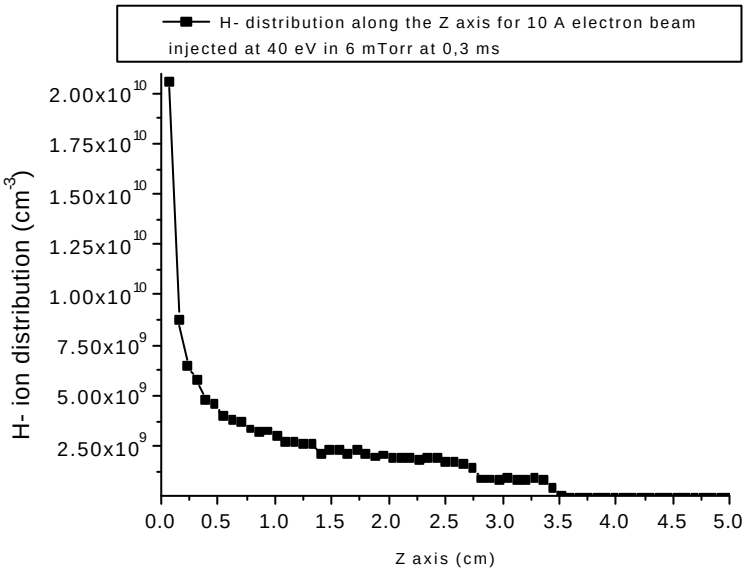

Figure 14: H- ion production vs the chamber length

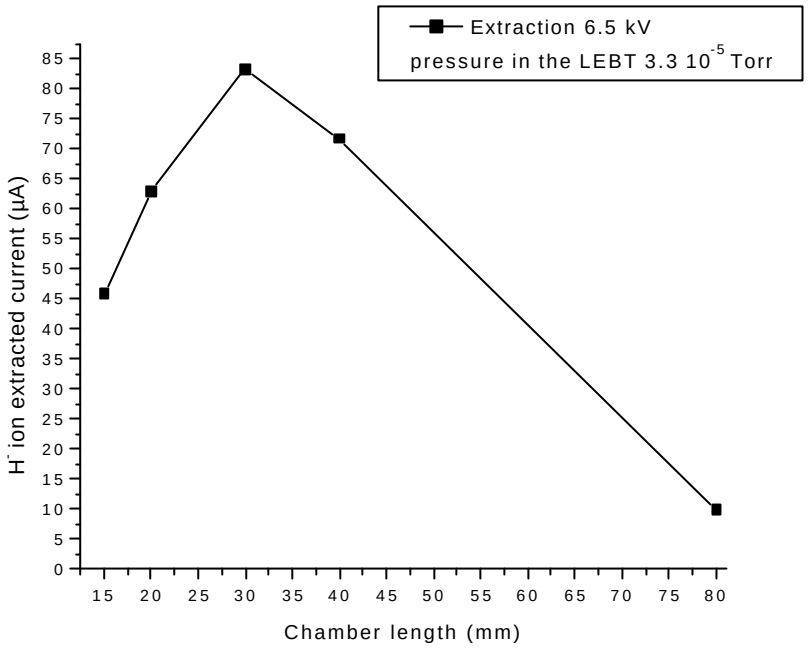

Figure 15: Experimental extracted current vs the chamber length

As shown in the Figure 12 the H⁻ ion production is constant along 3 cm with a chamber radius of 5 cm. If the assumption based on the non-extraction of H⁻ after 3 cm is correct, the present radius chamber (5 cm) is large enough the keep a high negative ion density along 3 cm. Indeed, the distribution depends on the boundary condition and a larger chamber can provide H- for a larger distance, but shorter is the radius higher is the injected power density. As it is well known, the injected power density plays an important role in the H⁻ production.

CONCLUSION

The code gives some interesting results, which are conforming to experimental measurement done in such a configuration by filament sources. It would help to define where the H ions are produced and place the extraction system at the right place. As it has been calculated an ideal system would be an extraction system placed after 3 cm from the electron injection. If the secondary chamber length were larger than 3 cm, it would not be as much efficient because of two reasons: H⁻ losses risk and electron energy efficiency not optimized enough. An ideal chamber radius of 5 cm has been determined as well. Experimental studies have been done in parallel with the ECR H⁻ ion source at CEA-Saclay. After introducing a simple stainless steel grid inside the chamber, the H⁻ current has been increased by a factor higher than 200. This grid stays intact after many months of non-stop work. Very promising results are expecting. It would be possible thanks to a double grid system to obtain an extraction and injecting system. Taking into account the calculations the ideal H⁻ source would be designed as shown in the Figure 16.

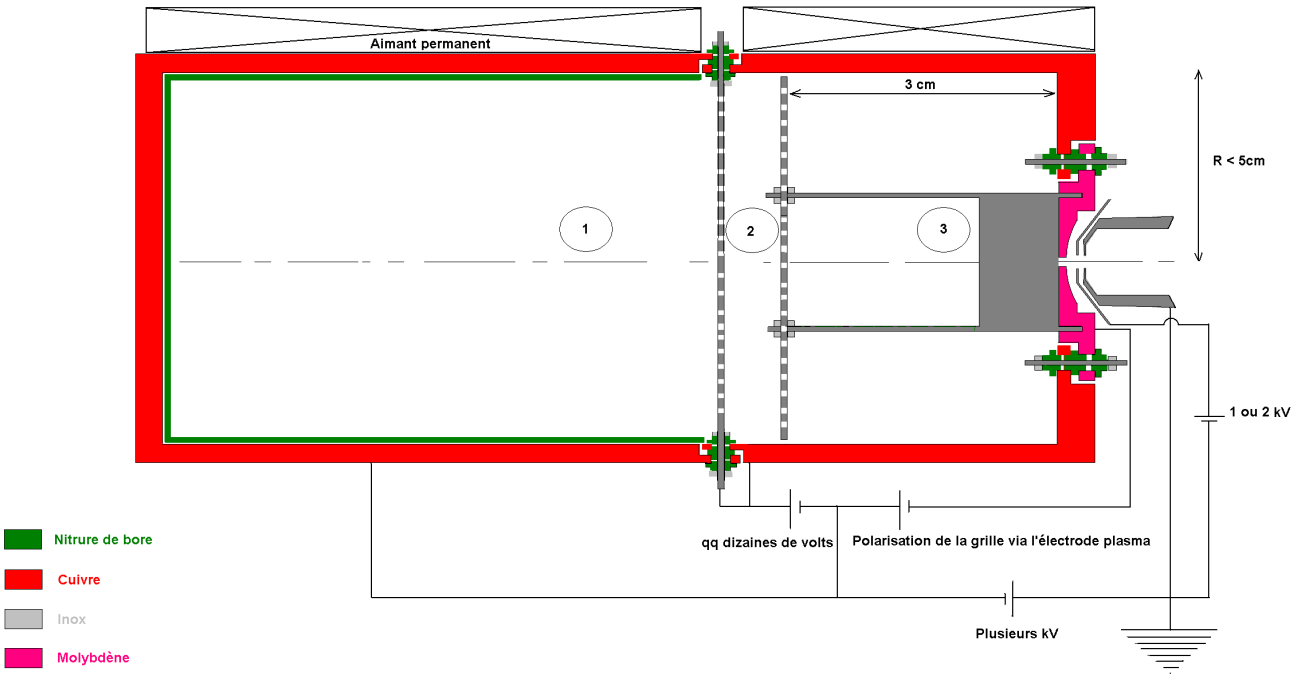

Figure 16: Source as it is thought to be the best.

ACKNOWLEDGMENTS

The authors want to thanks Ziane Kechidi, and Bruno Pottin who kindly offered they computer for running the code. A.France for his advices on the paper. Indeed, the technical staff at CEA Saclay for doing an amazing works on the source. Without them, there is no point to do this code: Francis Harrault and Yannick Gauthier.

REFERENCES

1 K. Benmeziane, R. Ferdinand, R. Gobin, G. Gousset, 'Study and preliminary results for a new type of ECR H ion source', Review of scientific instruments Vol 75(5) pp. 1729-1731. May 2004
2 R.Gobin, K.Benmeziane, O.Delferri re, R.Ferdinand, F.Harault and JD Sherman "The CEA/Saclay 2.45 GHz Microwave Ion Source for H^- Ion Production", AIP Conference proceedings 639,p177-183, 2002
3 R.Gobin, K.Benmeziane, O.Delferri re, R.Ferdinand, F.Harrault al."Observation of H^- Ions Extracted from a 2.45 Ghz Microwave Ion Source",EPAC Conference proceedings, Paris, France, p 1715, 2002.
4 R.Gobin, P-Y.Beauvais, K.Benmeziane, O.Delferri re, R.Ferdinand, F.Harrault, J-M.Lagniel, J.D.Sherman, "First plasma analysis of the CEA/Saclay ECR hydrogen negative ion source", review of scientific instruments vol73, number2, p983-985, feb2002.
5 R. Gobin, P-Y. Beauvais, K. Benmeziane, D. Bogard, G. Charruau, O. Delferri re, D. De Menezes, A. France, R. Ferdinand, Y. Gauthier, F. Harrault, J-L. Jannin, J-M. Lagniel, P. Matt i, A. Sinanna, J.D. Sherman, P. Ausset, S. Bousson, D. Gardes, B. Pottin, L. Celona, "Saclay High Intensity Light Ion Source Status" ,EPAC Conference proceedings, Paris, France, 2002 page1712-1716
6 M.B. Hopkins, M. Bacal, and W.G. Graham, "Enhanced volume production of negative ions in the post discharge of a multicusp hydrogen discharge", J. Appl. Phys. vol 70 (4), (15 August 1991), pp2009-2014
7 G.P.Arrighini, F.Biondi & C.Guidotti, Molecular Phys. vol 41 no 6 (1980) p1501-1514
8 M.A.P.Lima,T.L.Gibson, McKoy,& [PFTV92] W.M.Huo Phys.Rev.A vol38 (1988) p4527
9 J.R. Hiskes, Notas Physica 5 (1982) p348

10 V.P.Zhdanov&K.I.Zamarev,Catal.Rev.Sci.Eng V24 (1982) p373
11 C.Gorse, M.capitelli, M.Bacal, J.Bretagne, A.Lagana, Chem.Phys.117 (1987) p177-195.
12 J.Loureiro,C.M. Ferreira, J.Phys D :Appl.Phys (1989) 1680-1691
13 H.Tawara, Y.Itikawa, H.Nishimura and M.Yoshino, J.Phyis.Chem.ref.Data, V19,No3 (1990) p617-636
14 C.Gorse, M.Capitelli, M.Bacal,J.Bretagne, Chem.Phys V93 (1985) p1-12
15 D.Riz, J.Pamela, "Modeling of negative ion transport in a plasma source", Rev.Sci.Instrum. (1998) 69 p914-919
16 R. Gobin, P-Y. Beauvais, K. Benmeziane, O. Delferri re, R. Ferdinand, F. Harrault, J.D. Sherman, "Observation of H Ions Extracted from a 2.45 GHz Microwave Ion Source", EPAC Conference proceedings, Paris, France, 2002
17 D.L. Scharfetter and H. K. Gummel, IEEE Trans. Electron Device, vol 16, (1969), pp. 64-77